molecules

MDPI

*Article*

# Preparation of Perovskite-Type $LaMnO_3$ and Its Catalytic Degradation of Formaldehyde in Wastewater

**Qingguo Ma *, Pengcheng Huo, Kesong Wang, Ye Yuan, Songjiang Bai, Chentong Zhao and Wenzhuo Li**

Department of Chemistry and Chemical Engineering, Taiyuan Institute of Technology, Taiyuan 030008, China; h19935488662@outlook.com (P.H.); wks15364929146@163.com (K.W.); 19934924885@vip.163.com (Y.Y.); 18734854908@163.com (S.B.); 19935347014@163.com (C.Z.); 17789196649@163.com (W.L.)
* Correspondence: maqg@tit.edu.cn

**Abstract:** Formaldehyde (HCHO) is identified as the most toxic chemical among 45 organic compounds found in industrial wastewater, posing significant harm to both the environment and human health. In this study, a novel approach utilizing the Lanthanum-manganese complex oxide ($LaMnO_3$)/peroxymonosulfate (PMS) system was proposed for the effective removal of HCHO from wastewater. Perovskite-Type $LaMnO_3$ was prepared by sol-gel method. The chemical compositions and morphology of $LaMnO_3$ samples were analyzed through thermogravimetric analysis (TG), X-ray diffraction (XRD), X-ray photoelectron spectroscopy (XPS), and transmission electron microscopy (TEM). The effects of $LaMnO_3$ dosage, PMS concentration, HCHO concentration, and initial pH on the HCHO removal rate were investigated. When the concentration of HCHO is less than 1.086 mg/mL (5 mL), the dosage of $LaMnO_3$ is 0.06 g, and n(PMS)/n(HCHO) = 2.5, the removal rate of HCHO is more than 96% in the range of pH = 5–13 at 25 °C for 10 min. Compared with single-component $MnO_2$, the perovskite structure of $LaMnO_3$ is beneficial to the catalytic degradation of HCHO by PMS. It is an efficient Fenton-like oxidation process for treating wastewater containing HCHO. The $LaMnO_3$ promoted the formation of $SO_4^{\bullet -}$ and HO•, which sequentially oxidized HCHO to HCOOH and $CO_2$.

**Keywords:** formaldehyde; perovskite; catalytic oxidation; $LaMnO_3$; degradation



**Citation:** Ma, Q.; Huo, P.; Wang, K.; Yuan, Y.; Bai, S.; Zhao, C.; Li, W. Preparation of Perovskite-Type $LaMnO_3$ and Its Catalytic Degradation of Formaldehyde in Wastewater. *Molecules* **2024**, *29*, 3822. https://doi.org/10.3390/molecules29163822

Academic Editor: Albin Pintar

Received: 2 July 2024
Revised: 7 August 2024
Accepted: 9 August 2024
Published: 12 August 2024



## 1. Introduction

$ABO_3$ perovskite oxides containing transition metals are widely used, especially Lanthanum-containing manganate ($LaMnO_3$), which has attracted much attention due to its excellent performance in electrochemical [1–5] and catalytic reactions [6–9]. $LaMnO_3$ is widely used in catalytic oxidation reactions because of its catalytic activity, chemical stability, and high oxygen adsorption capacity [10]. In the catalytic oxidation of toluene, the conversion rate of toluene is over 90% at 330 °C because of the abundant oxygen vacancy in $LaMnO_3$ [11]. The catalyst performance and stability were tested in the oxidation of ethane; the experimental results showed that the conversion of ethane was promoted by the activation of C-H [12]. $LaMnO_3$ has obvious catalytic activity in the conversion rate of d-glucose to malonic acid, lactic acid, and levoacylpropionic acid. In the best conditions, 69.5 mol.% of lactic and levulinic acid were obtained [13]. The surface defects of $LaMnO_3$ were used to catalyze the oxidation of CO. The results showed that the O vacancy was conducive to the CO interaction, and the Mn vacancy was conducive to carbonate formation [14]. The band gap energies of $LaMnO_3$ in full spectrum (UV-Vis-IR) absorption is 0.75 eV. After Fe-Ni doping, the UV absorption of $La_{0.95}Fe_{0.025}Ni_{0.025}MnO_3$ showed a blue shift and the degradation time of high concentration Congo red dye (40 ppm) was shortened; the degradation time was 45 min [15]. Peroxymonosulfate (PMS) was activated with $LaMnO_3$ as a catalyst and the degradation rate of Ciprofloxacin antibiotics was 47.1% by Fenton-like catalytic oxidation. After the introduction of boron nitride quantum dots (BNQDs), the degradation of Ciprofloxacin antibiotics was significantly improved to 86.5% [16]. The

catalytic activity of Ag-, Y-, and Pd-doped $LaMnO_3$, and pure $LaMnO_3$ were studied for the methyl orange removal. The results showed that the catalytic activity of Ag-doped $LaMnO_3$ was slightly better than that of other catalysts. The maximum removal of methyl orange was 97% [17]. Undoped and Eu, Ho, Tb-doped $LaMnO_3$ materials were synthesized and studied in the removal rate of 17$\alpha$-ethynylestradiol from an aqueous environment. The best removal efficiency of 17$\alpha$-ethinylestradiol was 77% after 30 min of UV irradiation in the presence of LMO: Ho [18]. Because of its special crystal structure, perovskite has great application potential in catalytic hydrogen production [19], electrocatalysis [20], catalytic synthesis [21], catalytic combustion [22], electromagnetic wave absorbing material [23], and so on.

Formaldehyde (HCHO) is identified as the most toxic chemical among 45 organic compounds found in industrial wastewater, posing significant harm to both the environment and human health [24]. HCHO is widely used in various industrial manufacturing because of its high reactivity, resulting in toxic and harmful HCHO wastewater [25–28]. A large amount of HCHO wastewater was produced in the leather industry [29], preparation of urea-HCHO resin [30,31], and Phenol-HCHO resin production [32,33]. There are many methods for removing HCHO, including physical, chemical, biochemical, photochemical, electro-chemical, and thermal methods [34–36]. Studies have shown that physical adsorption is less costly, more efficient, and easier to implement than other methods [37,38]. However, there is no chemical reaction to mineralize the HCHO; HCHO is just adsorbed into the material and will still pollute the environment if desorbed. The practical application of biochemical and photo-chemical methods is commonly high cost, time consuming, or energy intensive [39,40]. In particular, HCHO has a strong biological resistance and toxicity to microorganisms, seriously restricting the application of biological treatment [41].

Chemical oxidation, particularly Fenton oxidation, is widely employed in wastewater treatment. Fenton reaction involves the reaction of $H_2O_2$ with $Fe^{2+}$ to produce ·OH radicals, which effectively oxidize pollutants in wastewater. However, the depletion of $Fe^{2+}$ and $H_2O_2$ ($Fe^{2+}$ is oxidized to $Fe^{3+}$) leads to the termination of the reaction. So Fenton oxidation requires the addition of catalysts and oxidants, and will produce iron sludge [42,43]. To overcome this problem, Fenton-like oxidations have been extensively explored as a more efficient strategy for removing pollutants from wastewater. When HCHO is degraded by electro-Fenton, HCHO is distributed in the electrolyte, while the free radicals are only distributed on the cathode surface. In addition, the short survival time ($10^{-6}$–$10^{-3}$ s) [44] of free radicals in water leads to the useless consumption of free radicals, thus reducing the reaction efficiency [45]. The Photo-Fenton system is superior to the Fenton system in the removal rate and complete mineralization rate of HCHO, because the presence of light regenerates $Fe^{3+}$ ions to $Fe^{2+}$, which can then react with more $H_2O_2$ [42]. Although the Photo-Fenton process is very effective in the treatment of HCHO, the pH value of the degradation reaction is limited to a certain range, and ultraviolet radiation is required [46]. C. Gao innovatively applied PMS activation technology to remove HCHO and produce hydrogen, when the initial HCHO concentration was 0.722 mol $L^{-1}$, the degradation rate of HCHO reached 30% [47]. J. Wei studied the degradation of nimesulide by $CoTiO_3/TiO_2$. The experimental results showed that the $CoTiO_3/TiO_2$ heterostructure promoted the targeted adsorption and activation of PMS, and the degradation rate of nimesulide was maintained above 91% [48]. In our previous experiments, we found that the complete removal of HCHO during degradation did not mean that HCHO was well treated because other contaminants, such as formic acid, were also produced [46,49]. Moussavi et al. used the catalytic advanced oxidation process and achieved 65.6% COD removal and 79% HCHO removal, but handling this technique was challenging [50].

It is important to obtain a catalyst that can simultaneously improve the ability of hydrogen peroxide or PMS, can be recycled, and has deactivation resistance for the oxidation of HCHO. This study investigates the efficiency of Fenton-like oxidation for treating wastewater containing HCHO. Two primary challenges must be addressed to facilitate the efficient degradation of HCHO through Fenton-like oxidation. Firstly, controlling the for-

mation rate of free radical OH is imperative. Secondly, ensuring sufficient contact between free radicals and HCHO is essential. In other words, the catalyst can adsorb HCHO and oxidants, and can catalyze the oxidant to produce free radicals.

## 2. Results

### *2.1. Draw HCHO Standard Curve*

Add 1 mL of acetylacetone solution (0.5% V/V%) and 30 μL of HCHO solution (1.086 mg/mL) to a 10 mL colorimetric tube, then fill it up with deionized water up to the scale line, shake well, and react for 3 min at 100 °C. After cooling down, use a UV-visible photometer to determine that the maximum absorption wavelength of the HCHO-acetylacetone solution is 414 nm as depicted in Figure 1.

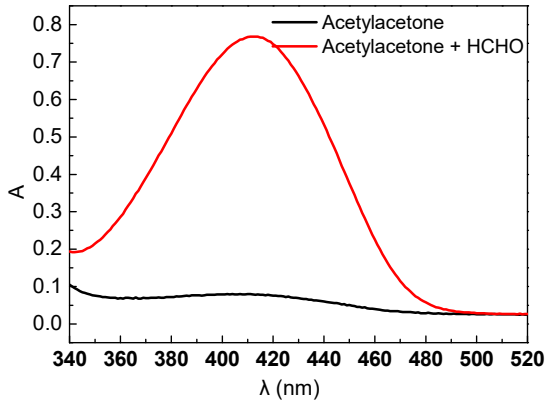


**Figure 1.** Wavelength scanning curve.

Figure 2 shows the standard curve of HCHO concentration and absorbance relationship. The linear fit within a range of 0.3–3 μg/mL was found to be 0.9966 for calculating HCHO concentration using this fitting curve.

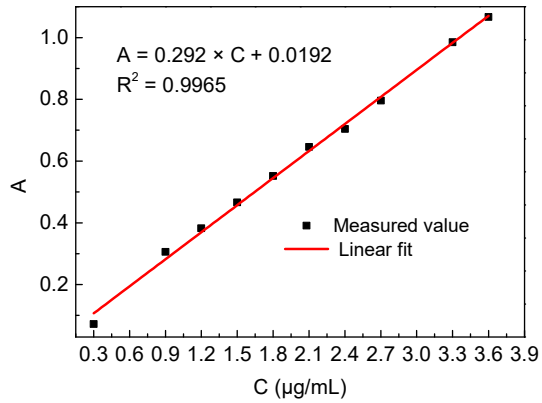


**Figure 2.** Standard curve of HCHO concentration and absorbance.

### *2.2. Catalyst Characterization*

As shown in Figure 3, the weight loss of the sample is more obvious at 200~400 °C, which may be due to the decomposition of excess citric acid. At 400~600 °C, the loss of weight is reduced, which may be manganese-lanthanum citrate composite decomposed at this temperature. To ensure the conversion of manganese lanthanum citrate composite into oxide, the calcination temperature was set at 700 °C.

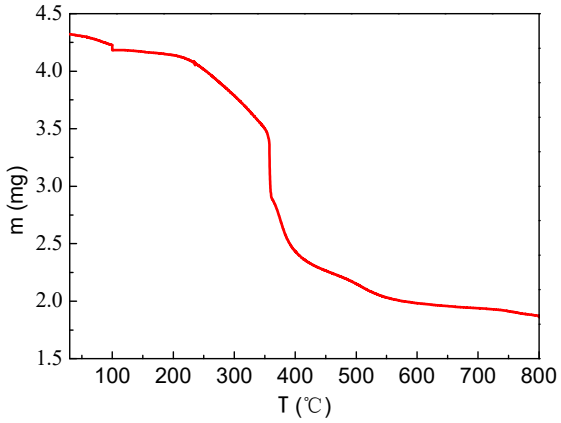


**Figure 3.** TG diagram of manganese-lanthanum citrate composite.

Peaks shown in Figure 4 (2θ = 22.88°, 32.76°, 40.2°, 46.92°, 52.7°, 58.1°, 68.6°, 77.8°) are in good agreement with the perovskite structure of $LaMnO_3$ (JCPDS No: 89-8775) [19,51,52]. The peaks at 2θ = 29.4°, 44.2°, and 73.2° ($LaMnO_3$-1, $LaMnO_3$-2, $LaMnO_3$-3 in Figure 4) may correspond to the crystallization peak of $MnO_2$ [7]. In addition, since the phase $La_2MnO_4$ is only stable above 1650 K and at low O partial pressures [52], the presence of $La_2MnO_4$ is further ruled out. With the increase in lanthanum content, the crystal diffraction peak intensity of $LaMnO_3$ increases, but the crystal peak of $La_2O_3$ does not appear. It is possible that $La_2O_3$ is highly dispersed in $LaMnO_3$ and does not form crystals or does not appear because of its low diffraction intensity.

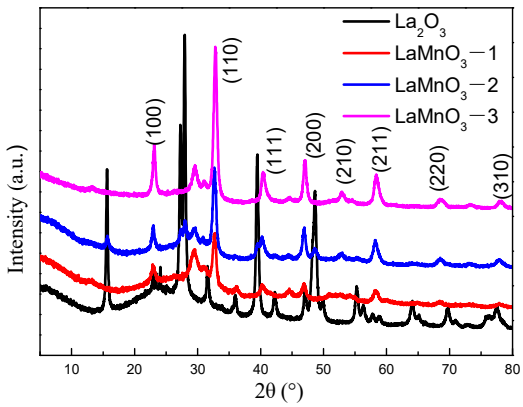


**Figure 4.** XRD patterns of Lanthanum-manganese complex oxides.

XPS of $LaMnO_3$-3 is shown in Figure 5. The peaks at 851.0 and 854.7 eV are assigned to $La3d_{3/2}$, and the peaks at 834.3 eV and 837.8 eV are assigned to $La3d_{5/2}$. The typical peaks are in correspondence to $La^{3+}$. The peaks at 641.9 eV (Mn $2p_{3/2}$) and 653.3 eV (Mn $2p_{1/2}$) correspond to $Mn^{3+}$, while the two peaks at 643.9 eV and 656.0 eV are ascribed to $Mn^{4+}$. In the lattice of $LaMnO_3$, $Mn^{3+}$ ions are the intrinsic valence of Mn, while $Mn^{4+}$ stems from the existence of La cation vacancies [4]. The removal rates of HCHO decreased from 96.65% to 90.3% and the catalytic efficiency only decreased by 6.35% after the catalyst was reused three times. The structure of $LaMnO_3$-3 before and after the catalytic oxidation reaction was characterized by XPS. As shown in Figure 5 the structure of $LaMnO_3$-3 has not changed after the catalytic oxidation reaction. The results show that the $LaMnO_3$ was stable.

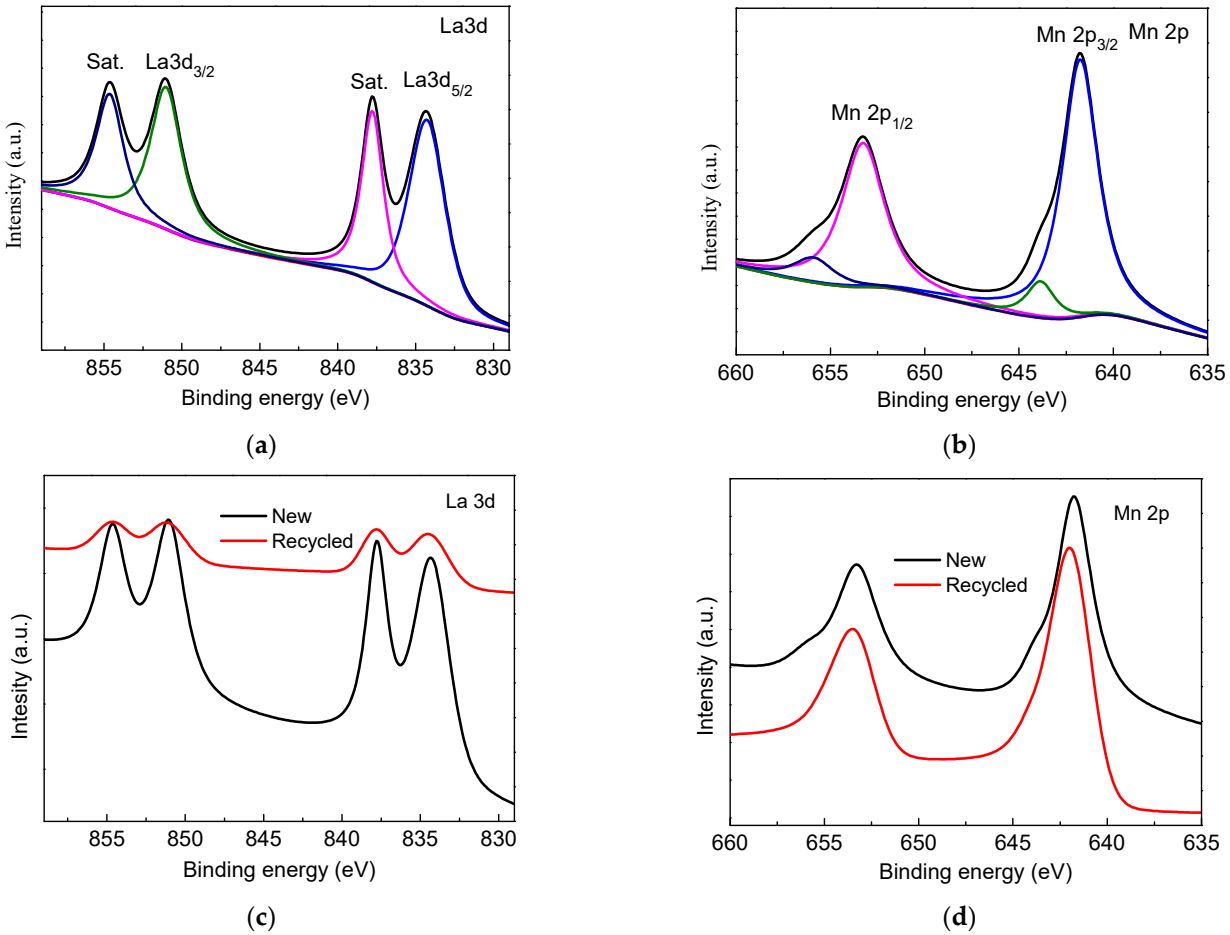


**Figure 5.** XPS of $LaMnO_3$ ((**a**): La3d, (**b**): Mn2p, (**c**): La 3d in recycled $LaMnO_3$-3, (**d**): Mn 3d in recycled $LaMnO_3$-3)).

The microstructure of $LaMnO_3$-3 was revealed in detail by TEM analysis. As shown in Figure 6, the particle size of the sample was about 20–50 nm. The lattice fringes of $LaMnO_3$-3 were obtained. The spacing of 0.274 nm was consistent with the (200) crystal plane in the X-ray diffraction spectra of the perovskite structure of $LaMnO_3$ [53].

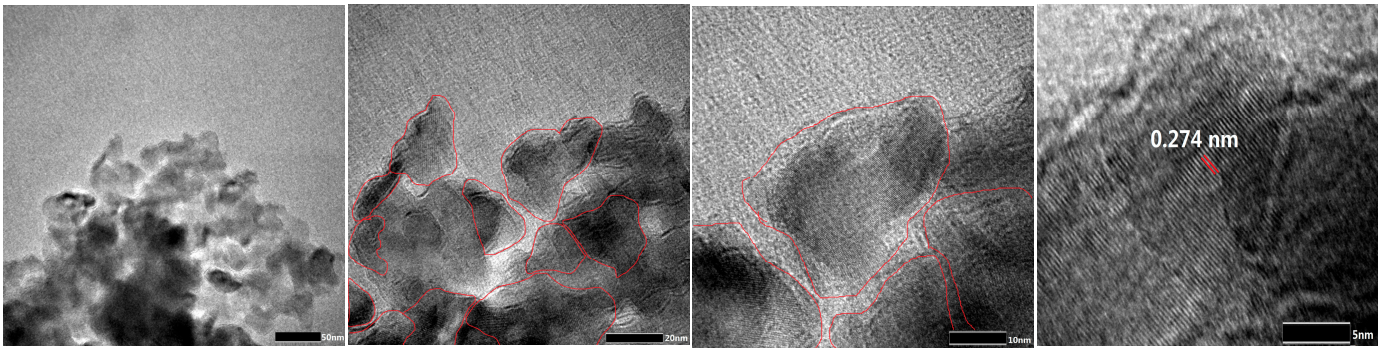


**Figure 6.** TEM images of $LaMnO_3$.

### *2.3. Catalytic Performance of $LaMnO_3$ for Degradation of HCHO*

The catalytic properties of $LaMnO_3$ with different lanthanum contents on the degradation of HCHO were investigated. Figure 7 shows that the removal rate of HCHO increased with the increase in lanthanum content in the catalyst. The adsorption of the catalysts on HCHO is weak, and the catalyst with the best adsorption is $MnO_2$. The maximum

adsorption rate of HCHO within 10 min is 18.27%, and the adsorption rate changes little after 2 min with the extension of time, which indicates that the removal of HCHO is mainly through catalytic oxidation reaction. Under the condition of no catalyst, using PMS as an oxidant, the removal rate of HCHO was 28.5%. Using $MnO_2$ as catalyst, the removal rate of HCHO was 64.69%, which was lower than the removal rate of formaldehyde using $LaMnO_3$ as catalyst. The removal rates of HCHO were 38.2% and 20.55%, respectively, when the same amount of hydrogen peroxide was used instead of PMS as the oxidant and $LaMnO_3$ or $MnO_2$ as the catalyst to catalyze the degradation of HCHO. The potassium iodide-starch test paper test showed that $MnO_2$ promoted the decomposition of hydrogen peroxide and reduced the oxidant in the reaction system. The same test method confirmed that $LaMnO_3$ promoted the decomposition of hydrogen peroxide. Although $LaMnO_3$ can also catalyze the decomposition of PMS, it is much slower than its catalytic decomposition of hydrogen peroxide. Hydrogen peroxide breaks down in 6 min, while PMS takes 90 min. The results indicate that the perovskite structure of $LaMnO_3$ is beneficial to the catalytic degradation of HCHO by PMS. As can be seen from Figure 8 the removal rate of HCHO increased with the increase in catalyst dosage. However, when the amount of catalyst increased to 0.06 g, the removal rate of HCHO increased slightly with the increase in catalyst dosage. The results indicated that $LaMnO_3$ catalyzes PMS to generate $SO_4\bullet^-$ and $SO_4\bullet^-$ was more stable than HO●. Therefore, increasing catalyst dosage does not affect the stability of $SO_4\bullet^-$.

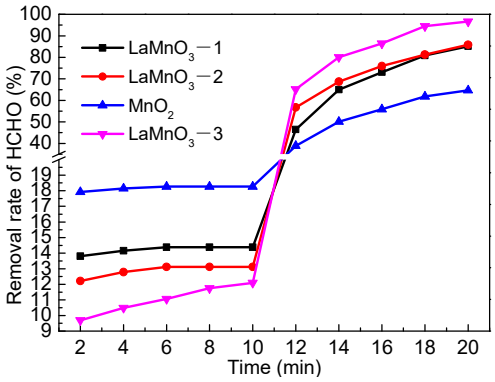


| Pseudo-first-order | Catalyst composition | | | |
|---|---|---|---|---|
| | $LaMnO_3-1$ | $LaMnO_3-2$ | $LaMnO_3-3$ | $MnO_2$ |
| K ($min^{-1}$) | 0.1589 | 0.1054 | 0.2982 | 0.0684 |
| $R^2$ | 0.9922 | 0.9397 | 0.9862 | 0.9779 |

**Figure 7.** Effect of catalyst composition on the removal rate of HCHO (5 mL HCHO solution (1.086 mg/mL), catalyst 0.06 g, add PMS 0.13 g after 10 min, 25 °C).

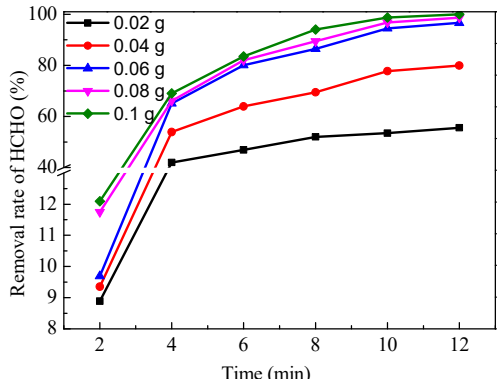


| Pseudo-first-order | Catalyst dosage | | | | |
|---|---|---|---|---|---|
| | 0.02 g | 0.04 g | 0.06 g | 0.08 g | 0.1 g |
| K ($min^{-1}$) | 0.0332 | 0.0827 | 0.2982 | 0.408 | 0.7029 |
| $R^2$ | 0.955 | 0.9153 | 0.9862 | 0.9799 | 0.9351 |

**Figure 8.** Effect of catalyst dosage on the removal rate of HCHO (5 mL HCHO solution (1.086 mg/mL), add PMS 0.13 g after 2 min, 25 °C).

The effect of different PMS dosages on the removal rate of HCHO was tested. As can be seen from Figure 9, the removal rate of HCHO increased with the increase in PMS dosage. However, when the amount of PMS increased to 0.13 g, the removal rate of HCHO increased slightly with the increase in PMS dosage. This is because increasing the amount of PMS without changing the amount of catalyst slightly changes the production of $SO_4\bullet^-$.

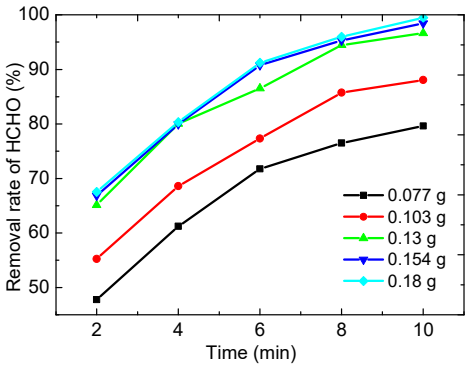


| Pseudo-first-order | PMS dosage | | | | |
|---|---|---|---|---|---|
| | 0.077 g | 0.103 g | 0.13 g | 0.154 g | 0.18 g |
| K ($min^{-1}$) | 0.1191 | 0.136 | 0.2982 | 0.3782 | 0.4946 |
| $R^2$ | 0.974 | 0.9302 | 0.9862 | 0.9827 | 0.9223 |

**Figure 9.** Effect of PMS dosage on the removal rate of HCHO (5 mL HCHO solution (1.086 mg/mL), catalyst 0.06 g, 25 °C).

As shown in Figure 10, when the concentration of HCHO was more than 1.629 mg/mL, the removal rate of HCHO was less than 80%. It is possible that the amount of $SO_4\bullet^-$ produced under the same catalyst dosage may affect the degradation of HCHO. When the amount of catalyst was constant, the amount of $SO_4\bullet^-$ produced was limited even if the amount of oxidant was increased. Therefore, when the concentration of HCHO was more than 1.629 mg/mL, the effects of the amount of catalyst and PMS on the conversion of HCHO need to be further investigated. The COD values of the HCHO solutions with different concentrations were measured by a water quality analyzer, and the COD removal rates were calculated. When the concentration of HCHO was 0.272 mg/mL, 0.543 mg/mL, 1.086 mg/mL, 1.629 mg/mL, and 2.172 mg/mL, the COD removal rates were 83.5%, 80.3%, 74.4%, 52.3%, and 40.8%, respectively. These results suggest that PMS cannot fully mineralize HCHO. The production of formic acid results in a low COD removal rate.

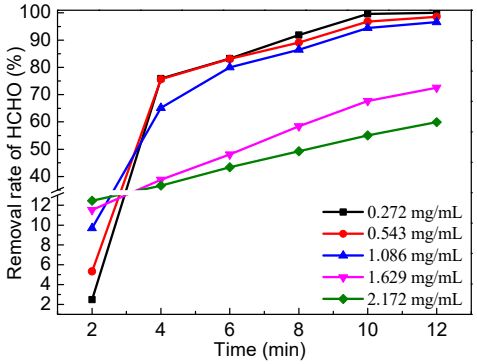


| Pseudo-first-order | HCHO concentration | | | | |
|---|---|---|---|---|---|
| | 0.272 mg/mL | 0.543 mg/mL | 1.086 mg/mL | 1.629 mg/mL | 2.172 mg/mL |
| K ($min^{-1}$) | 0.7393 | 0.3317 | 0.2982 | 0.104 | 0.0573 |
| $R^2$ | 0.905 | 0.8929 | 0.9862 | 0.9946 | 0.9998 |

**Figure 10.** Effect of HCHO concentration on the removal rate of HCHO (n(PMS)/n(HCHO) = 2.5, catalyst 0.06 g, add PMS after 2 min, 25 °C).

At pH 1, 3, 5, 7, 9, 11, and 13, the removal rate of HCHO was 76.06%, 93.72%, 99.39%, 96.65%, 97.77%, 99.5%, and 100%, respectively. The removal rate of formaldehyde is lower under acidic conditions. It may be that hydrogen ions hinder the formation of $SO_4\bullet^-$ and •OH under acidic conditions. Therefore, fewer free radicals can participate in the degradation of formaldehyde under acidic conditions [54].

## 3. Discussion

When 1 mL of deionized water was added to the reaction system, the removal rate of HCHO was 98.65%, and when 1 mL of tert-butyl alcohol was added, the removal rate of formaldehyde decreased to 85.41%. Although the radical quenching agent of tert-butanol inhibited the degradation of HCHO, the decrease degradation rate of HCHO is not very large. The results show that $LaMnO_3$ catalyzed PMS to generate $SO_4\bullet^-$ and HO•, and $SO_4\bullet^-$ was dominant.

The changes in the composition of the HCHO solution before and after the catalytic oxidation reaction were analyzed by HPLC. After the catalytic oxidation of HCHO, two peaks appeared, at 2.93 min and 3.17 min. When HCHO was replaced with water and the same amount of $LaMnO_3$-3 and PMS were added, only one peak appeared at 2.93 min. The peak appeared at 3.17 min and was verified with a formic acid solution.

$LaMnO_3$-3 calcined in air at 700 °C was further calcined at 900 °C and 1100 °C for 2 h, respectively. $LaMnO_3$-3 calcined at 900 °C and 1100 °C were marked as $LaMnO_3$-900 and $LaMnO_3$-1100. The catalytic degradation of HCHO by $LaMnO_3$-900 and $LaMnO_3$-1100 was investigated (5 mL HCHO solution (1.086 mg/mL), catalyst 0.02 g, PMS 0.13 g, 25 °C, 10 min). The removal rates of HCHO were 43.77% and 42.39%. Under the same conditions, the removal rate of HCHO was 55.57 for the $LaMnO_3$-3 calcined at 700 °C. These results suggest that with the increase in calcination temperature, the removal rate of HCHO decreased. We speculate that the charge of manganese changes at elevated temperatures [55,56]. Since $Mn^{4+}$ is stabilized in the perovskite phase [52], the increase in calcination temperature leads to the conversion of $Mn^{3+}$ to $Mn^{4+}$. Under oxidizing conditions, the formation of OH is due to the charge change in Mn in $LaMnO_3$, which changes from $Mn^{3+}$ to $Mn^{4+}$.

Based on the above experimental results, a possible reaction pathway for removing HCHO with PMS over $LaMnO_3$ was proposed. The reaction pathway was presented in Figure 11. The oxidation of HCHO is a Fenton-like oxidation reaction. The $LaMnO_3$ promoted the formation of $SO_4\bullet^-$ and HO•. HCHO was oxidized to HCOOH and $CO_2$ by $SO_4\bullet^-$ and HO•.

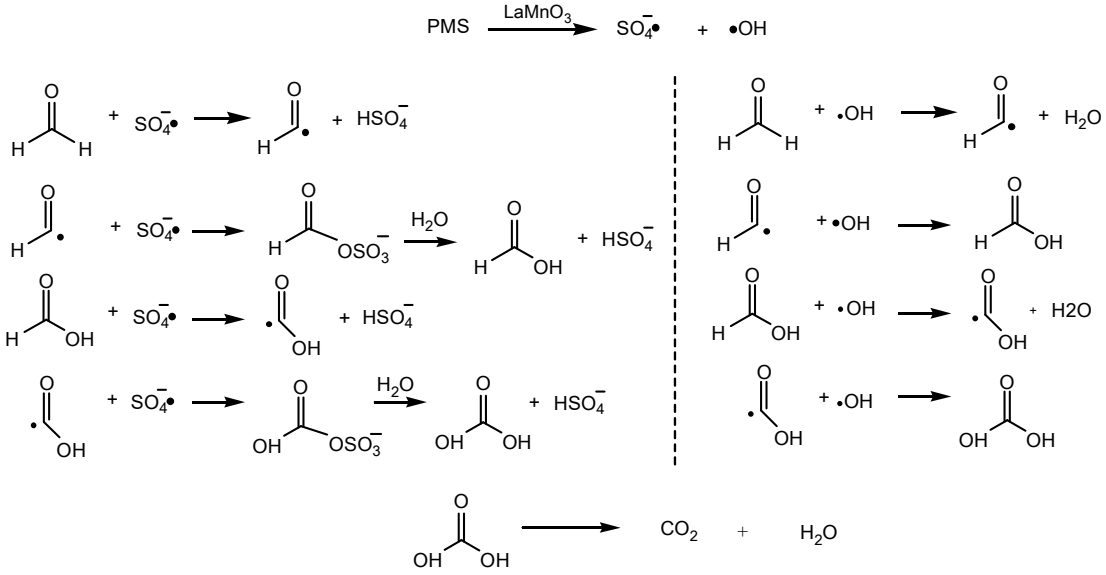


**Figure 11.** A possible reaction pathway for removing HCHO with PMS over $LaMnO_3$.

## 4. Materials and Methods

### *4.1. Preparation of HCHO Standard Solution*

Add HCHO solution (approximately 1 mg/mL, 20 mL), sodium hydroxide solution (1 mol/L, 15 mL), and iodine solution (0.05 mol/L, 20 mL) to a iodine flask, shake well, and add sulfuric acid solution (0.05 mol/L, 20 mL) after 15 min. Then react for another 15 min, and titrate with sodium thiosulfate standard solution until the solution is pale yellow. Add starch indicator (1 mL) and continue titrating until the blue color is just faded. The volume of the sodium thiosulfate solution consumed is $V_2$. Using 20 mL of deionized water instead of 20 mL of HCHO solution, titrated with standard sodium thiosulfate by the same method, the consumption volume is $V_1$. The concentration of HCHO standard solution was calculated using Equation (1).

$$C = (V_1 - V_2) \times C_{Na_2S_2O_3} \times 15/20. \quad (1)$$

Based on the volume of sodium thiosulfate standard solution consumed, the concentration of HCHO standard solution was 1.086 mg/mL.

### *4.2. Draw the HCHO Standard Curve*

Next, add 0.3 mL, 0.6 mL, 0.9 mL, 1.2 mL, 1.5 mL, 1.8 mL, 2.1 mL, 2.4 mL, 2.7 mL, and 3.0 mL HCHO standard solution (10.86 μg/mL) to 10 colorimetric tubes (10 mL), then add deionized water to scale line. Shake well, and react for 3 min at 100 °C. After cooling, the photometer was used to measure the absorbance of the different concentrations of HCHO solution at 414 nm, and the standard curve of HCHO concentration-absorbance was drawn.

### *4.3. Preparation of Catalyst*

Then 2.948 g of citric acid was added to 10 mL of deionized water and 3.567 g of lanthanum nitrate and 1.432 g of manganese nitrate solution (50%) were added to 10 mL of deionized water. The citric acid solution is then added to the mixed solution of lanthanum nitrate and manganese nitrate. The solution was stirred at 80 °C and evaporated into the gel. The gel was dried in an oven at 100 °C for 4 h, and then transferred to a muffle furnace calcined in air at 700 °C for 4 h then naturally cooled to room temperature. Then the sample materials with different ratios of lanthanum and manganese were prepared by the same process. The molar ratios of lanthanum nitrate to manganese nitrate were 1:1, 2:1, and 3:1, marked as $LaMnO_3$-1, $LaMnO_3$-2, and $LaMnO_3$-3.

### *4.4. Catalyst Characterization*

The thermal decomposition temperature of manganese-lanthanum citrate composite salt was determined by a thermogravimetric analyzer (TGA4000). The sample was determined in air with a flow rate of 20 mL/min. The temperature rising rate and range were 10 °C/min and 30~800 °C, respectively. The phase composition and crystal structure of the synthesized Lanthanum-manganese complex oxides ($LaMnO_3$) were determined by X-ray diffraction analysis (XRD, Rigku, Smartlab, Tokyo, Japan), X-ray photoelectron spectrometer (XPS, ThermoFisher, ESCALAB 250Xi, Waltham, MA, USA), and the transmission electron microscope (TEM, JEOL, JEM-F200, Tokyo, Japan).

### *4.5. Catalytic Activity Experiment*

The catalytic activity and stability of Lanthanum-manganese complex oxides were researched towards the degradation of HCHO with PMS as an oxidant. In a catalytic activity process, under stirring conditions, 0.06 g $LaMnO_3$ was added into a 5 mL HCHO solution (1.086 mg/mL). Then, 0.13 g PMS (85 mM in the reaction solution) was added to the above mixture solution and kept at 25 °C for 10 min. Samples are taken from the mixture every 2 min during the reaction. The catalyst and PMS in the sample were removed by 0.45 μm filter membrane and sodium thiosulfate, respectively. At last, the sample solution was added to the acetylacetone solution to measure the absorbance and calculate the degradation rate of HCHO.

### *4.6. Analysis of Degradation Products*

After the catalytic oxidation reaction (HCHO standard solution (5 mL), 0.06 g $LaMnO_3$, 0.13 g PMS, 10 min), the degradation product was detected by an iChrom5000 high-performance liquid chromatography (HPLC) with diode array detector (DAD). The test conditions are as follows. Column: SinoChrom ODS-BP 5 um 4.6 × 150 mm, Column temperature: 30 °C, Mobile Phase: v (Methanol)/v (0.5% phosphoric acid solution) = (90/10), flow rate: 0.6 mL/min, Detection Wavelength: 210 nm.

In addition, the mixture of 5 mL water, 0.06 g $LaMnO_3$, 0.13 g PMS, and HCOOH solution (11.2 mg/mL) was also detected by HPLC under the same test conditions.

### *4.7. Measurement of Chemical Oxygen Demand (COD)*

The COD of the HCHO standard solution before and after the catalytic oxidation reaction was measured by a water quality analyzer (DGB-401). The test conditions are as follows. Take 2 mL of samples of HCHO standard solution (before and after the catalytic oxidation reaction) to a pre-configured COD detection reagent, cover the colorimetric tube tightly, shake and mix well. This solution was cooled after reacting at 150 °C for 2 h and tested for COD at 470 nm.

## 5. Conclusions

Lanthanum-manganese complex oxides were prepared by the sol-gel method. The perovskite structure was determined by XRD and TEM analysis, and the perovskite structure of $LaMnO_3$ is beneficial to the catalytic degradation of HCHO by PMS compared with single-component $MnO_2$. The catalytic activity of $LaMnO_3$ was investigated for the removal of HCHO from the aqueous solution. It is an efficient Fenton-like oxidation process for the treatment of wastewater containing HCHO. The $LaMnO_3$ promoted the formation of $SO_4\bullet^-$ and HO•, which sequentially oxidized HCHO to HCOOH and $CO_2$. Because the decomposition rate of $H_2O_2$ catalyzed by $LaMnO_3$ is too fast and the HO• life is too short, it is not suitable for catalytic degradation of formaldehyde. The removal rate of HCHO increased with the increase in lanthanum content in the catalyst, catalyst dosage, and PMS dosage. The maximum removal of HCHO was 100% (5 mL HCHO solution (1.086 mg/mL), catalyst 0.1 g, PMS 0.13 g, 25 °C, 10 min). At pH 1, 3, 5, 7, 9, 11, and 13, the removal rate of HCHO was 76.06%, 93.72%, 99.39%, 96.65%, 97.77%, 99.5%, and 100%, respectively. The removal rate under acidic conditions is low because hydrogen ions hindered the formation of $SO_4\bullet^-$ and •OH. When the concentration of HCHO is less than 1.086 mg/mL, and the amount of catalyst is constant, the removal rate of HCHO is more than 96%. However, when the concentration of HCHO is more than 1.629 mg/mL, the effects of the amount of catalyst and PMS on the conversion of HCHO need to be further investigated. The quenching tests proved that the removal of HCHO is through a radical pathway, and the key oxidant is $SO_4\bullet^-$. The HO• life is too short to react with HCHO.

**Author Contributions:** Conceptualization and methodology: Q.M.; formal analysis and investigation: Q.M., P.H., K.W., Y.Y., S.B., C.Z. and W.L.; writing—original draft preparation: Q.M. and P.H.; writing—review and editing: Q.M., P.H. and K.W.; funding acquisition: Q.M., P.H. and K.W.; resources: Q.M. All authors have read and agreed to the published version of the manuscript.

**Funding:** This study was supported by the National Natural Science Fund of China (grant no. 22072105).

**Institutional Review Board Statement:** Not applicable.

**Informed Consent Statement:** Not applicable.

**Data Availability Statement:** No new data were created.

**Conflicts of Interest:** The authors declare no conflicts of interest.

## References

1. Zheng, J.; Zhao, H.; Guo, X.; Jin, X.; Wang, L.; Dong, S.; Chen, J. Enhanced Electrochemical Performance of $LaMnO_3$ Nanoparticles by Ca/Sr Doping. *Coatings* **2024**, *14*, 20. [CrossRef]
2. Sfirloaga, P.; Taranu, B.; Poienar, M.; Vlazan, P. Addressing electrocatalytic activity of metal-substituted lanthanum manganite for the hydrogen evolution reaction. *Surf. Interfaces* **2023**, *39*, 102881. [CrossRef]
3. Aljurays, R.K.; Loucif, A.; Albadri, A.M. Synthesis of $LaXO_3$ (X = Fe, Mn, Cr, Ni) Thin Films Using a Simple Spin Coating Set-Up for Resistive Switching Memory Devices. *Electronics* **2023**, *12*, 4141. [CrossRef]
4. Zhu, T.; Zheng, K.; Wang, P.; Cai, X.; Wang, X.; Gao, D.; Yu, D.; Chen, C.; Liu, Y. A new zinc-ion battery cathode with high-performance: Loofah-like lanthanum manganese perovskite. *J. Colloid Interface Sci.* **2022**, *610*, 796–804. [CrossRef] [PubMed]
5. Shukla, A. Distinct dominant dielectric relaxation mechanisms in $CaCu_3Ti_4O_{12}$–$LaMO_3$ (M = Mn and Fe) perovskite oxide solid solution. *J. Solid State Chem.* **2023**, *325*, 124182. [CrossRef]
6. Wang, J.; Liang, X.; Xing, Z.; Chen, H.; Li, Y.; Song, D.; He, F. Ce-Doped $LaMnO_3$ Redox Catalysts for Chemical Looping Oxidative Dehydrogenation of Ethane. *Catalysts* **2023**, *13*, 131. [CrossRef]

7. Li, L.; Liu, Y.; Liu, J.; Zhou, B.; Guo, M.; Liu, L. Catalytic Degradation of Toluene over $MnO_2$/$LaMnO_3$: Effect of Phase Type of $MnO_2$ on Activity. *Catalysts* **2022**, *12*, 1666. [CrossRef]
8. Li, C.; Chen, X.; Zhang, Q.; Zhang, C.; Li, Z.; Niu, J.; He, Z.; Xing, Q.; Tian, Z.; Ma, W.; et al. Novel porous perovskite composite $CeO_2$@$LaMnO_3$/3DOM $SiO_2$ as an effective catalyst for activation of PMS toward oxidation of urotropine. *Adv. Powder Technol.* **2022**, *33*, 103802.
9. Nie, Y.; Zhou, H.; Tian, S.; Tian, X.; Yang, C.; Li, Y.; Tian, Y.; Wang, Y. Anionic ligands driven efficient ofloxacin degradation over $LaMnO_3$ suspended particles in water due to the enhanced peroxymonosulfate activation. *Chem. Eng. J.* **2022**, *427*, 130998. [CrossRef]
10. Evans, C.D.; Bartley, J.K.; Taylor, S.H.; Hutchings, G.J.; Kondrat, S.A. Perovskite Supported Catalysts for the Selective Oxidation of Glycerol to Tartronic Acid. *Catal. Lett.* **2023**, *153*, 2026–2035. [CrossRef]
11. Wu, P.; Chen, T.; Jin, X.; Zhao, S.; Chong, Y.; Li, Y.; Lin, J.; Li, A.; Zhao, Y.; Qiu, Y. Quenching-induced surface modulation of perovskite oxides to boost catalytic oxidation activity. *J. Hazard. Mater.* **2022**, *433*, 128765. [CrossRef] [PubMed]
12. Jin, F.; Cheng, X.; Wan, T.; Gong, J.; Liang, T.; Wu, G. The role of modified manganese perovskite oxide for selective oxidative dehydrogenation of ethane: Not only selective $H_2$ combustion but also ethane activation. *Catal. Commun.* **2022**, *172*, 106531. [CrossRef]
13. Scelfo, S.; Geobaldo, F.; Pirone, R.; Russo, N. Catalytic wet air oxidation of d-glucose by perovskite type oxides (Fe, Co, Mn) for the synthesis of value-added chemicals. *Carbohydr. Res.* **2022**, *514*, 108529. [CrossRef] [PubMed]
14. Tapia, P.J.; Cao, Y.; Gallego, J.; Guillén, J.M.O.; Morgan, D.; Espinal, J.F. CO Oxidation Catalytic Effects of Intrinsic Surface Defects in Rhombohedral $LaMnO_3$. *Chemphyschem* **2022**, *23*, e202200152. [CrossRef]
15. Wahba, M.A.; Sharmoukh, W.; Yakout, S.M.; Khalil, M.S. Fast and full spectrum sunlight photocatalysts: Fe/Co or Ni implanted multiferroic $LaMnO_3$. *Opt. Mater.* **2022**, *124*, 111973. [CrossRef]
16. Balta, Z.; Simsek, E.B. Boosted photocatalytic hydrogen production and photo-Fenton degradation of ciprofloxacin antibiotic over spherical LaMnO3 perovskites assembled boron nitride quantum dots. *Int. J. Hydrogen Energy* **2023**, *48*, 26781–26794. [CrossRef]
17. Sfirloaga, P.; Ivanovici, M.; Poienar, M.; Ianasi, C.; Vlazan, P. Investigation of Catalytic and Photocatalytic Degradation of Methyl Orange Using Doped $LaMnO_3$ Compounds. *Processes* **2022**, *10*, 2688. [CrossRef]
18. Merkulov, D.Š.; Vlazan, P.; Poienar, M.; Bognár, S.; Ianasi, C.; Sfirloaga, P. Sustainable removal of 17$\alpha$-ethynylestradiol from aqueous environment using rare earth doped lanthanum manganite nanomaterials. *Catal. Today* **2023**, *424*, 113746. [CrossRef]
19. Zhan, M.; Fang, M.; Li, L.; Zhao, Y.; Yang, B.; Min, X.; Du, P.; Liu, Y.; Wu, X.; Huang, Z. Effect of Fe dopant on oxygen vacancy variation and enhanced photocatalysis hydrogen production of $LaMnO_3$ perovskite nanofibers. *Mater. Sci. Semicond. Process* **2023**, *166*, 107697. [CrossRef]
20. Zheng, H.; Zhang, Y.; Wang, Y.; Wu, Z.; Lai, F.; Chao, G.; Zhang, N.; Zhang, L.; Liu, T. Perovskites with Enriched Oxygen Vacancies as a Family of Electrocatalysts for Efficient Nitrate Reduction to Ammonia. *Small* **2023**, *19*, 2205625. [CrossRef]
21. Alcamand, H.; Oliveira, H.; Gabriel, J.; Bruziquesi, C.; Oliveira, L.; Gonçalves, B.; Victória, H.; Krambrock, K.; Houmard, M.; Nunes, E. Environmentally friendly synthesis of imine using $LaMnO_3$ as a catalyst under continuous flow conditions. *Mater. Lett.* **2022**, *316*, 132053. [CrossRef]
22. Qin, J.; Zhao, P.; Meng, J.; Zuo, S.; Wang, X.; Zhu, W.; Liu, W.; Liu, J.; Yao, C. Surface exposure engineering on $LaMnO_3$@$Co_2MnO_4$ for high-efficiency ethane catalytic combustion. *Appl. Surf. Sci.* **2024**, *653*, 159393. [CrossRef]
23. Liu, X.; He, L.; Han, G.; Sheng, J.; Yu, Y.; Yang, W. Design of rich defects carbon coated $MnFe_2O_4$/$LaMnO_3$/$LaFeO_3$ heterostructure nanocomposites for broadband electromagnetic wave absorption. *Chem. Eng. J.* **2023**, *476*, 146199. [CrossRef]
24. Chen, Y.; He, L.; Li, J.; Zhang, S. Multi-criteria design of shale-gas-water supply chains and production systems towards optimal life cycle economics and greenhouse gas emissions under uncertainty. *Comput. Chem. Eng.* **2018**, *109*, 216–235. [CrossRef]
25. Yamada, M.; Funaki, S.; Miki, S. Formaldehyde interacts with RNA rather than DNA: Accumulation of formaldehyde by the RNA-inorganic hybrid material. *Int. J. Biol. Macromol.* **2019**, *122*, 168–173. [CrossRef] [PubMed]
26. Xu, Q.; Sun, H.; Ren, M.; Kong, F. A novel cellulose-based fluorescent probe for the quantitative detection of HCHO in real food samples and living cells. *Ind. Crop. Prod.* **2023**, *204*, 117406. [CrossRef]
27. Kou, Y.; Zhao, H.; Cui, D.; Han, H.; Tong, Z. Formaldehyde toxicity in age-related neurological dementia. *Ageing Res. Rev.* **2022**, *73*, 101512. [CrossRef] [PubMed]
28. Li, T.; Chen, F.; Zhou, Q.; Wang, X.; Liao, C.; Zhou, L.; Wan, L.; An, J.; Wan, Y.; Nan, L. Unignorable toxicity of formaldehyde on electroactive bacteria in bioelectrochemical systems. *Environ. Res.* **2020**, *183*, 109143. [CrossRef]
29. Yusuf, M.A.; Agustina, L. The potential application of photocatalytic processes in the processing of wastewater in the leather industry: A Review. *IOP Conf. Ser. Earth Environ. Sci.* **2023**, *1253*, 012025. [CrossRef]
30. Mei, X.; Ma, M.; Guo, Z.; Shen, W.; Wang, Y.; Xu, L.; Zhang, Z.; Ding, Y.; Xiao, Y.; Yang, X.; et al. A novel clean and energy-saving system for urea-formaldehyde resin wastewater treatment: Combination of a low-aeration-pressure plate membrane-aerated biofilm reactor and a biological aerated filter. *J. Environ. Chem. Eng.* **2021**, *9*, 105955. [CrossRef]
31. Pu, H.; Han, K.; Dai, R.; Shan, Z. Semi-liquefied bamboo modified urea-formaldehyde resin to synthesize composite adhesives. *Int. J. Adhes. Adhes.* **2022**, *113*, 103061. [CrossRef]
32. Pervova, I.G.; Klepalova, I.A.; Lipunov, I.N. Recycling Phenolic Wastewater from Phenol-Formaldehyde Resin Production. *IOP Conf. Ser. Earth Environ. Sci.* **2021**, *666*, 042032. [CrossRef]

33. Manna, S.; Bobde, P.; Roy, D.; Sharma, A.K.; Mondal, S.J. Separation of iodine using neem oil-cashew nut shell liquid based-phenol formaldehyde resin modified lignocellulosic biomatrices: Batch and column study. *J. Taiwan Inst. Chem. E* **2021**, *122*, 98–105. [CrossRef]
34. Wang, H.; Song, T.; Li, Z.; Qiu, J.; Zhao, Y.; Zhang, H.; Wang, J. Exceptional High and Reversible Ammonia Uptake by Two Dimension Few-layer $BiI_3$ Nanosheet. *ACS Appl. Mater. Interfaces* **2021**, *13*, 25918–25925. [CrossRef] [PubMed]
35. Wang, X.; Feng, Z.; Xiao, B.; Zhao, J.; Ma, H.; Tian, Y.; Pang, H.; Tan, L. Polyoxometalate-based metal–organic framework-derived bimetallic hybrid materials for upgraded electrochemical reduction of nitrogen. *Green Chem.* **2020**, *22*, 6157–6169. [CrossRef]
36. Bahador, F.; Foroutan, R.; Esmaeili, H.; Ramavandi, B. Enhancement of the chromium removal behavior of Moringa oleifera activated carbon by chitosan and iron oxide nanoparticles from water. *Carbohydr. Polym.* **2021**, *251*, 117085. [CrossRef]
37. Khaleghi, H.; Esmaeili, H.; Jaafarzadeh, N.; Ramavandi, B. Date seed activated carbon decorated with CaO and $Fe_3O_4$ nanoparticles as a reusable sorbent for removal of formaldehyde. *Korean J. Chem. Eng.* **2022**, *39*, 146–160. [CrossRef]
38. An, S.; Zhao, Z.; Bu, J.; He, J.; Ma, W.; Lin, J.; Bai, R.; Shang, L.; Zhang, J. Multi-Functional Formaldehyde-Nitrate Batteries for Wastewater Refining, Electricity Generation, and Production of Ammonia and Formate. *Angew. Chem. Int. Ed.* **2024**, *63*, e202318989. [CrossRef] [PubMed]
39. Chen, B.; Bao, S.X.; Zhang, Y.M.; Ren, L.Y. A novel and sustainable technique to precipitate vanadium from vanadium-rich solutions via efficient ultrasound irradiation. *J. Clean. Prod.* **2022**, *339*, 130755. [CrossRef]
40. Tan, Y.; Yin, C.; Zheng, S.; Di, Y.; Sun, Z.; Li, C. Design and controllable preparation of $Bi_2MoO_6$/attapulgite photocatalyst for the removal of tetracycline and formaldehyde. *Appl. Clay Sci.* **2021**, *215*, 106319. [CrossRef]
41. Santos, S.; Jones, K.; Abdul, R.; Boswell, J.; Paca, J. Treatment of wet process hardboard plant VOC emissions by a pilot scale biological system. *Biochem. Eng. J.* **2007**, *37*, 261–270. [CrossRef]
42. Athikaphan, P.; Wongsanga, K.; Klanghiran, S.; Lertna, N.; Neramittagapong, A.; Rood, S.C.; Nijpanich, S.; Neramittagapong, S. Degradation of formaldehyde by photo-Fenton process overn-ZVI/$TiO_2$ catalyst. *Environ. Sci. Pollut. R.* **2023**, *30*, 90397–90409. [CrossRef] [PubMed]
43. Bello, M.M.; Raman, A.A.A.; Asghar, A. A Review on Approaches for Addressing the Limitations of Fenton Oxidation for Recalcitrant Wastewater Treatment. *Process Saf. Environ. Prot.* **2019**, *126*, 119–140. [CrossRef]
44. Wang, L.L.; Lan, X.; Peng, W.Y.; Wang, Z.H. Uncertainty and misinterpretation over identification, quantification and transformation of reactive species generated in catalytic oxidation processes: A review. *J. Hazard. Mater.* **2021**, *408*, 124436. [CrossRef] [PubMed]
45. Lai, S.; Zhao, H.; Qu, Z.; Tang, Z.; Yang, X.; Jiang, P.; Wang, Z. Promotion of formaldehyde degradation by electro-Fenton: Controlling the distribution of ·OH and formaldehyde near cathode to increase the reaction probability. *Chemosphere* **2022**, *307*, 135776. [CrossRef] [PubMed]
46. Ma, Q.; Shi, S.; Yang, F.; Zhang, X. Removal of formaldehyde in water with low concentration of hydrogen peroxide catalyzed by lanthanum-silicon oxide composite. *Desalin. Water Treat.* **2023**, *300*, 101–106. [CrossRef]
47. Gao, C.; Feng, X.; Yi, L.; Wu, X.; Zheng, R.; Zhang, G.; Li, Y. Peroxymonosulfate activation based on $Co_9S_8$@N−C: A new strategy for highly efficient hydrogen production and synchronous formaldehyde removal in wastewater. *J. Mater. Sci. Technol.* **2022**, *127*, 256–267. [CrossRef]
48. Wei, J.; Chen, J.; Li, F.; Han, D.; Gong, J. Anchoring $CoTiO_3$/$TiO_2$ heterostructure on fiber network actuates flow-through Fenton-like oxidation: Electronic modulation and rapid pollutants degradation. *Sep. Purif. Technol.* **2024**, *336*, 126231. [CrossRef]
49. Ma, Q.; Hao, Y.; Xue, Y.; Niu, Y.; Chang, X. Removal of Formaldehyde from Aqueous Solution by Hydrogen Peroxide. *J. Water Chem. Technol.* **2022**, *44*, 297–303. [CrossRef]
50. Moussavi, G.; Yazdanbakhsh, A.; Heidarizad, M. The removal of formaldehyde from concentrated synthetic wastewater using $O_3$/MgO/$H_2O_2$ process integrated with the biological treatment. *J. Hazard. Mater.* **2009**, *171*, 907–913. [CrossRef]
51. Kumar, R.D.; Sampath, S.; Thangappan, R.; Gosu, N.R.; Manthrammel, M.A.; Shkir, M. Citric acid mediated hydrothermal synthesis of $LaMn_{1-x}Fe_xO_3$ nanoparticles for visible light driven photocatalytic applications. *J. Mater. Sci. Mater. Electron.* **2024**, *35*, 2. [CrossRef]
52. Grundy, A.N.; Chen, M.; Hallstedt, B.; Gauckler, L.J. Assessment of the La-Mn-O System. *J. Phase Equilib. Diff.* **2005**, *26*, 131–151. [CrossRef]
53. Mao, M.; Xu, J.; Li, Y.; Liu, Z. Hydrogen evolution from photocatalytic water splitting by $LaMnO_3$ modified with amorphous $CoS_x$. *J. Mater. Sci.* **2020**, *55*, 3521–3537. [CrossRef]
54. He, Y.; Qian, J.; Wang, P.; Wu, J.; Lu, B.; Tang, S.; Gao, P. Acceleration of levofloxacin degradation by combination of multiple free radicals via $MoS_2$ anchored in manganese ferrite doped perovskite activated PMS under visible light. *Chem. Eng. J.* **2022**, *431*, 133933. [CrossRef]

55. Hauback, B.C.; Fjellvag, H.; Sakai, N. Effect of Nonstoichiometry on Properties of $La_{1-t}MnO_{3+\delta}$. *J. Solid State Chem.* **1996**, *124*, 43–51. [CrossRef]
56. Kekade, S.S.; Yadav, P.A.; Thombare, B.R.; Dusane, P.R.; Phase, D.M.; Choudhari, R.J.; Pati, S.I. Effect of sintering temperature on electronic properties of nanocrystalline $La_{0.7}Sr_{0.3}MnO_3$. *Mater. Res. Express* **2019**, *6*, 096108. [CrossRef]